Molecular Catalysis xxx (xxxx) xxx–xxx

Contents lists available at ScienceDirect

Molecular Catalysis

journal homepage: www.elsevier.com/locate/mcat

Limonene oxyfunctionalization over Cu-modified silicates employing hydrogen peroxide and *t*-Butyl hydroperoxide: Reaction pathway analysis

Virginia M. Vaschetti[a], Analía L. Cánepa[a], Deicy Barrera[b], Karim Sapag[b], Griselda A. Eimer[a], Sandra G. Casuscelli[a,*]

[a] Centro de Investigación y Tecnología Química, UTN-CONICET, Facultad Regional Córdoba, Maestro López esq. Cruz Roja Argentina, S/N, CP 5016, Córdoba, Argentina
[b] Laboratorio de Sólidos Porosos, INFAP-CONICET, Universidad Nacional de San Luis, Avenida Ejército de los Andes, 950, CP 5700, San Luis, Argentina

ARTICLE INFO

Keywords:
Cu-MCM
Limonene
H_2O_2
Oxidation
TBHP

ABSTRACT

Limonene oxidation over Cu-nanostructured mesoporous materials was studied. Three solids with different copper content were synthesized employing the template-ion exchange method, and physically-chemically analyzed by a multi-technical characterization. The performance of the molecular sieves as catalysts in the liquid phase oxyfunctionalization of limonene, employing hydrogen peroxide (H_2O_2) or *t*-butyl hydroperoxide (TBHP) as oxidants was evaluated. All synthesized Cu-MCM materials were active in the reaction. The obtained results showed that the used oxidant had an important influence on the products distribution under the employed conditions. With H_2O_2, compounds of high added value such as limonene oxide, carveol and carvone were mainly obtained. Meanwhile, with TBHP, limonene hydroperoxide turned out to be the major product. Finally, a reaction mechanism was proposed for each oxidant.

1. Introduction

(+)-Limonene is a monocyclic terpene present in large quantities in the essential oils of various citrus fruits. Commercially, it is obtained mainly as a by-product of the orange juice industry from the waste orange peel, which contains approximately 3.8 wt.% of this terpene (on a dry basis) [1]. Its readily availability and inexpensiveness explain the interest in limonene as a green platform chemical to obtain high value added products [2,3].

The oxidation of limonene allows obtaining several oxygenated derivatives with important applications as organic synthesis intermediaries. Most of these products are used in the food, agrochemical, cosmetic and pharmaceutical industries [4]. The high reactivity of the limonene molecule is mainly associated with the presence of two double bonds located in the positions 1–2 and 8–9 [3]. Under oxidation conditions, both unsaturated bonds can be oxidized to form the corresponding oxides. Moreover, several others compounds, such as carveol, carvone, glycols, among others, can also be obtained as products. Normally, more than one reaction mechanism competes to form different oxygenated derivatives. This places special importance on controlling the reaction selectivity. Two mayor reaction pathways can be identified: homolytic (via free radicals) and heterolytic (via peroxometal or oxometal) which are mainly related to the metal used as catalyst [5,6].

In previous works, the oxidation of limonene has been studied by our research group employing Ti-MCM [7] and Cu(II) complex heteropolytungstates supported on alumina [8], obtaining good conversions and selectivities towards oxidation products. Recently, several materials containing different transition metals ions have successfully proven to catalyze the liquid phase oxidation of limonene. Charbonneau and Kaliaguine [9] have reported a limonene conversion of 80% with a selectivity of 79% to 1,2-limonene oxide over Ti-SBA-16 after 24 h of reaction. The system employed acetonitrile as a solvent and TBHP as the oxidant in a limonene/TBHP molar ratio of 0.54. In the past few years, Wróblewska and others have worked in the limonene oxidation over various titanium-silicate catalysts (TS-2, Ti-Beta, Ti-MCM-41, and Ti-MWW) [4,10,11]. Different experiments at autogenic and atmospheric pressure, employing H_2O_2 and TBHP in a limonene/oxidant molar ratio of 0.5 and 1, showed that a variety of products could be obtained depending on the reaction conditions. Ciriminna et al. [12] investigated the photocatalytic properties of crystalline TiO_2 for limonene epoxidation under solar light irradiation. They found that the selectivity to desired product notably varied with the reaction time and the pre-reaction treatment applied to TiO_2. Młodzik et al. [13] examined the performance of several activated carbons modified with different iron contents in the limonene oxidation with H_2O_2 and TBHP,

* Corresponding author.
E-mail address: scasuscelli@frc.utn.edu.ar (S.G. Casuscelli).

https://doi.org/10.1016/j.mcat.2018.11.005
Received 13 July 2018; Received in revised form 3 November 2018; Accepted 5 November 2018

employing a limonene/oxidant molar ratio of 0.5. As products limonene glycol, carveol, carvone, and perillyl alcohol were obtained. Their research showed that product selectivity depended on the used oxidant and the metal load in the catalyst. Becerra and coworkers investigated the oxidation of limonene with TBHP employing iron hexadecachlorinated phthalocyanine immobilized on modified silica [2]. Using a limonene/TBHP molar ratio of 0.38, a limonene conversion of 74% was obtained after 23 h with 10% selectivity to carvone. In the same way, other reports on limonene oxidation have also been developed evaluating the activity of zeolitic supports modified with transition metals complexes [14,15]. The above mentioned catalytic systems show the high complexity of the limonene oxidation process. All the results demonstrate that the reaction selectivity is heavily influenced by multiple factors such as the used oxidant, type of catalyst and metal load, solvent employed, reaction temperature and limonene/oxidant ratio.

We have focused on testing a catalytic system that combines the simplicity of a mesoporous silicate such as MCM-41, with the low cost, high redox potential, environmentally benign nature and readily availability of copper [16,17]. It is known that there is a wide variety of methods that can be used to modify M41S type supports with different transition metals. All Cu-MCM-41 materials evaluated in this work were synthesized employing the template-ion exchange (TIE) method. This method allows a simple functionalization of the MCM-41 surface by deposition of highly dispersed metal species [18,19]. Moreover, many efforts have been made to optimize the synthesis of M41S materials [20,21]. It has been reported that the replacement of tetraethylammonium hydroxide (TEAOH) for NaOH in the synthesis of the MCM-41 results in a better structure in the final solid [22]. Therefore, this modification could represent an improvement over other Cu-TIE molecular sieves previously reported [23]. In the present study, the copper modified mesoporous molecular sieves were evaluated as catalysts on the liquid phase oxidation of limonene with H_2O_2 and TBHP. With the aim to understand the obtained catalytic results, the synthesized materials were characterized by XRD, UV–vis-DR, ICP and N_2 adsorption-desorption at 77 K. Moreover, a reaction mechanism was proposed to explain the products distribution observed for each oxidant.

2. Materials and methods

2.1. Catalyst synthesis

The pure siliceous matrix (MCM-41) was synthesized following method B reported in [22] by Elías *et al.* Cetyltrimethylammonium bromide (CTAB, Merck 99%) was used as surfactant (Surf), tetraethoxysilane (TEOS, Aldrich 98%) as silicon source and 2 M aqueous solution of NaOH for hydrolysis and pH adjustment. The molar composition of the starting gel was: Surf/Si = 0.12, NaOH/Si = 0.5 and H_2O/Si = 132. In a typical synthesis, CTAB was dissolved at 313 K in NaOH and distilled water. After this solution was cooled to room temperature, the silicon source was quickly added. The resulting mixture was stirred vigorously for 4 h at 298 K, and then for an additional 3 h at 343 K. Finally, the resulting white solid was washed, filtered and dried overnight at 333 K. For its characterization, a part of the MCM-41 was desorbed at 773 K in N_2 atmosphere for 6 h (heating rate 2 K/min), and then calcined at the same temperature in air for another 6 h to remove the surfactant.

The copper modified materials were synthesized with different copper loadings using the template-ion exchange method [24]. 3.16 g of the undesorbed MCM-41 containing approximately 52.5 wt.% of surfactant was added to a $Cu(NO_3)_2.2.5H_2O$ (*J.*T.Baker 99.7%) solution which concentration corresponded to the nominal metal loading. The mixture was stirred at room temperature for 1 h and then placed under autogenous pressure at 353 K in a steel reactor lined with teflon for 20 h. Then the light blue solids were filtered, dried, desorbed and calcined, following the same procedure previously described for the MCM-41. The resulting brown materials were named Cu-TIE(x), where the “x” refers to the solids nominal metal loading in wt.%.

2.2. Characterization techniques

The X-ray diffraction patterns (XRD) were taken at low and high angles between 2°–8° and 20°–80° using an X-Pert Pro PANalitic Diffractometer with copper Kα radiation of 1.5418 Å. The lattice parameter of the hexagonal unit cell (a_0) was calculated according to the equation $a_0 = (2/\sqrt{3})d_{100}$, where d_{100} refers to the interplanar distance calculated based on the position of the most intense diffraction line at low angle. N_2 adsorption-desorption isotherms data at 77 K were obtained using a manometric instrument Micromeritics, ASAP 2000, where the samples were previously degassed at 573 K for 12 h. The specific surface (S_{BET}) was determined by the Brunauer-Emmett-Teller method (BET), the total pore volume (V_{TP}) was estimated at a relative pressure of 0.98, and the primary mesoporous volume (V_{MPP}) was calculated by the a_S-plot method using the standard (PSD) was evaluated employing the Functional Theory of Non-Localized Density (NLDFT) based on the adsorption branch, and the N_2 kernel at 77 K on silica for cylindrical pores. XPS measurements were performed on a SPECS Multi-technique spectrometer, equipped with a dual X-ray source (Mg/Al) and a hemi-spherical analyzer PHOIBOS 150 in fixed analyzer transmission mode (FAT). The spectra were recorded with a step energy of 30 eV, employing a Mg anode operated at 200 W. The pressure during the measurement was lower than 1.10^{-9} mbar. The samples were pressed, supported on the instrument sample holders, subjected to vacuum (10^{-2} mbar) for 10 min at 473.15 K. Subsequently, ultra-high vacuum was applied for at least two hours before analyzing. The UV–vis-DR spectra were collected in air at room temperature with a UV–vis-DR Spectrophotometer with an integrated sphere for diffuse reflectance Jasco V-650. The range of wavelengths used was 200 nm – 900 nm and the data were converted employing the Kubelka-Munk equation. The total copper content in the final solid was determined by Atomic Absorption (AA) using a Shimadzu AA7000.

2.3. Limonene oxidation

Limonene oxidation reactions, with H_2O_2 or TBHP, were carried out under vigorous stirring in a batch system that consisted of a reflux condenser connected to a glass reactor submerged in a bath at 343 K for 5 h. In a typical reaction, limonene (Lim, R(+)-Fluka 98%) was used as reagent, H_2O_2 (Cicarelli 30% in water) or TBHP (Aldrich 70% in water) as oxidant (molar ratio Lim/oxidant 2:1) and the Cu-TIE(x) as a reaction catalyst (14.3 g/L). The solvent used in all cases was acetonitrile (AcN, Sintorgan 99.5%) in a 15:1 M ratio with limonene. Some reactions were carried out under nitrogen atmosphere and others using a radical scavenger. To create a nitrogen atmosphere, several cycles of vacuum-nitrogen income were performed to the reaction system while the reacting mixture was kept at 273 K. After the selected conditions were reached, the reactor was submerged in the bath at 343 K, and the nitrogen atmosphere was maintained during the 5 h of reaction. When a radical scavenger was used, 2,6-di-tertbutyl-4-methylphenol (BHT) was added at the beginning of the reaction in a quantity that was equal to 8% of the initial limonene mmols. In all cases, the reaction progress was recorded by taking samples at different times through a reactor lateral tabulation. The aliquots were filtered and analyzed by gas chromatography (GC) using an Agilent 7820 chromatograph equipped with an HP-1 capillary column and a FID detector. The percentage of each component in the reaction sample was calculated using the area normalization method employing response factors. Both, H_2O_2 and TBHP were determined by iodometric titration. The conversion (X) of substrate (Lim) and oxidant (Ox), the selectivity (S) for product “i” and the turnover number (TON), at reaction time "t" were calculated according to Eqs. (1)-(4). In the corresponding equations, “n” represents the mmols of limonene, oxidant or product “i”, while the subscript “o”

indicates the beginning of the reaction. TON calculation is carried out considering all the copper present in the synthesized materials acts as an active reaction site.

$$X_{Lim,t}(\%)=\frac{n_{Lim,o}-n_{Lim,t}}{n_{Lim,o}}\times 100 \quad (1)$$

$$X_{Ox,t}(\%)=\frac{n_{Ox,o}-n_{Ox,t}}{n_{Ox,o}}\times 100 \quad (2)$$

$$S_{i,t}(\%)=\frac{n_{i,t}}{n_{Lim,o}-n_{Lim\,t}}\times 100 \quad (3)$$

$$TON_t=\frac{n_{Lim,o}-n_{Lim,t}}{\text{Cu moles in the catalyst}}\times 100 \quad (4)$$

Identification of the reaction products was carried out by direct comparison with standards and gas chromatography with mass spectrometry (GC–MS). The equipment used for GC–MS analysis was a Clarus SQ8 Perkin Elmer equipped with an Elite 5MS capillary column. The data was acquired through the TurboMass 6.1.0 program in Full Scan mode, from $m/z = 40$ to $m/z = 350$. The signals identification was made by comparison of the obtained mass spectra with the ones found in the libraries of the NIST MS Search 2.0 program. Mass spectral data (m/z/intensity ratio) for the identified products are the following: Limonene oxide: 41/52, 43/100, 67/69, 79/40, 81/35, 93/41, 94/47, 108/37, 109/30. Limonene diepoxide: 41/22, 43/100, 55/25, 67/27, 71/12, 79/18, 93/15, 95/30, 107/21. Limonene glycol: 41/38, 43/87, 58/29, 67/40, 68/21, 69/34, 71/100, 82/29, 108/31, 152/22. Carveol: 41/55, 43/32, 55/47, 69/37, 83/40, 84/100, 109/56, 134/50. Carvone: 41/17, 53/11, 54/50, 82/100, 93/23, 106/11, 107/14, 108/27. Perillaldehyde: 41/42, 53/46, 67/54, 68/100, 77/37, 79/60, 93/35, 107/44, 150/33. Limonene hydroperoxide: 41/46, 43/36, 55/45, 82/63, 84/46, 91/42, 93/79, 107/78, 109/100.

3. Results and discussion

3.1. Material characterization

The low-angle XRD patterns of the siliceous matrix and copper modified materials synthesized in this study are shown in Fig. 1A. The pure matrix exhibits an intense reflection at 2.43° which corresponds to the distance between the (100) structure planes. It also shows two other less intense signals at 4.22° and 4.83° representative of the (110) and (200) planes, respectively. This observed diffraction pattern is characteristic of well-ordered MCM-41 materials with a long-range one-dimensional pore system in hexagonal arrangement [25]. Since the copper modified solids have a similar diffraction pattern to that observed for the pure matrix, it is possible to affirm that the copper-containing samples possess a typical MCM-41 structure and that the long structural regularity of the matrix is maintained even after the template-ion exchange treatment. However, it is important to note that the increase in copper loading causes a small broadening of the first peak and a mild intensity decrease, mainly of the first signal. This could indicate a certain loss of periodicity regarding the mesoporous structure. At the same time, the diffraction patterns of the Cu-TIE samples are slightly displaced towards lower angles, which may be consistent with the copper incorporation in the siliceous structure [26].

Fig. 1B presents the support and Cu-TIE samples high angle diffraction patterns after their calcination in air. At $2\theta \sim 23°$, all solids show the typical wide signal corresponding to amorphous silica. For the three copper modified materials, other two signals located at around 35.4° and 38.6° can also be identified. These peaks may be assigned to crystalline copper(II) oxide (CuO) according to the pure oxide high angle pattern shown in the same figure. As it can be observed by the relative intensities of the peaks, a higher copper loading favors the formation of bigger oxide species located on the external surface of the support. No signals related to crystalline copper(I) oxide (Cu_2O) were observed [27].

Fig. 2A shows the N_2 adsorption-desorption isotherms at 77 K for the samples under study. These isotherms are type IV according to the IUPAC classification, which is typical of mesoporous materials. It should also be noted that these catalysts present a higher mesoporosity than the support (MCM-41) probably due to the employed synthesis procedure. All samples exhibit a high structural ordering level due to the capillary condensation stage is well defined. Furthermore, after capillary condensation in the primary mesoporous, there is a plateau (in samples Cu-TIE(1%) and Cu-TIE(2%)) suggesting that there is no significant presence of secondary mesoporosity. Regarding the isotherm shape of sample Cu-TIE(5%), the sharp increase at relative pressures

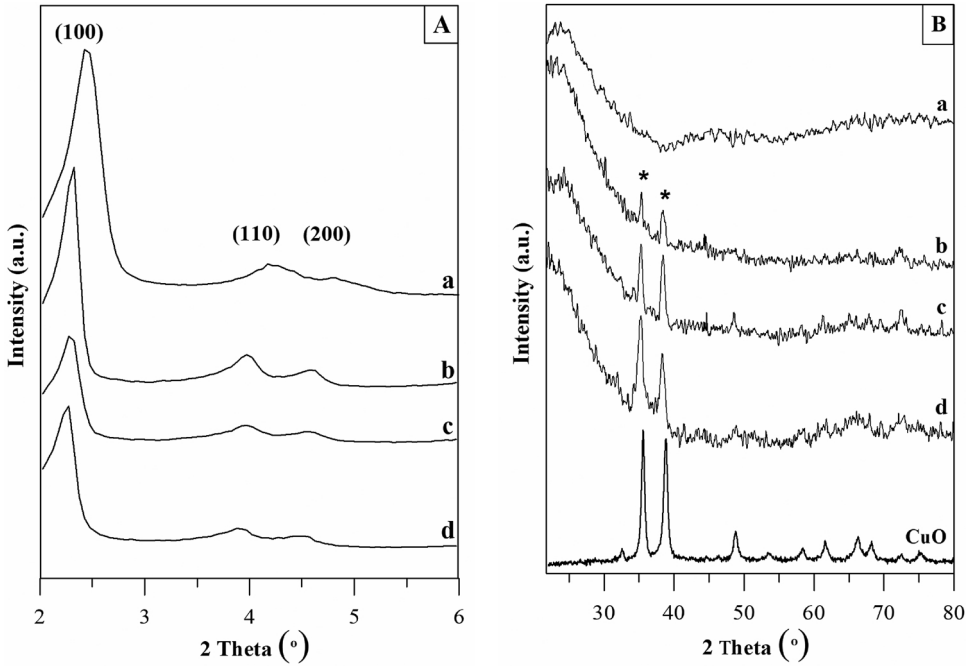

Fig. 1. XRD patterns of the samples. **A**: at low angle. **B**: at high angle, (*) CuO. **a**: MCM-41, **b**: Cu-TIE(1%), **c**: Cu-TIE(2%), **d**: Cu-TIE(5%).

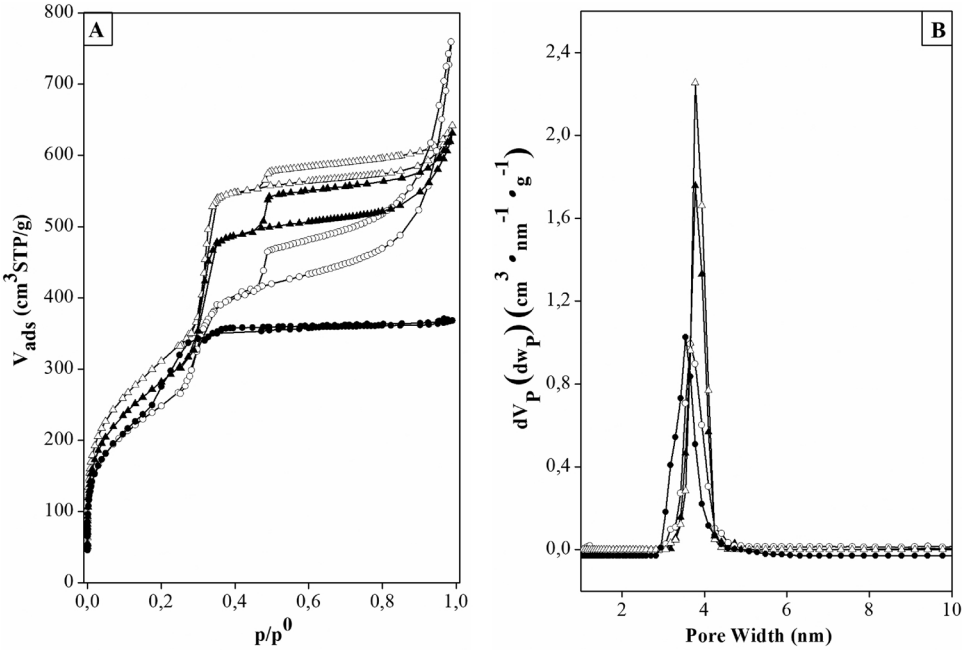

Fig. 2. A: Nitrogen adsorption – desorption isotherms at 77 K. **B**: NLDFT pore size distribution of the samples. (Δ) Cu-TIE(1%), (▲) Cu-TIE(2%), (○) Cu-TIE(5%), (●) MCM-41.

close to 1 is likely due to an agglomeration of particles outside of the MCM-41 pore structure owing to the Cu content. This is reflected in the formation of a small secondary mesoporosity in this sample. Pore size distributions for all materials are shown in Fig. 2B. Unimodal PSD with mesoporous sizes between 3.5 nm – 3.8 nm can be observed. However, a decrease in pore volumes and a small shift in the pore size are observed as the copper content increases. This may be related to an agglomeration of particles on the mesoporous support surface.

Table 1 gathers the textural and chemical properties of the synthesized samples. The pore width (w_p) was determined from the N_2 adsorption data as it was previously explained. The lattice parameter of the hexagonal unit cell (a_0) was calculated employing Bragg's Law and the wall thickness (t_w) was estimated as the difference between a_0 and w_p. As it can be seen, a reduction in the specific surface of the solids can be detected as the metal content increases. This could be related to the presence of bigger copper oxide particles (as the ones detected by XRD) formed on the external surface of the support. These particles could be blocking some of the MCM-41 pores, therefore causing a decrease in S_{BET}. For the sample with the highest metal content, a slight increase in t_w can also be detected. This result could confirm the presence of copper nanoclusters dispersed inside the MCM-41 channels, besides their agglomeration on the external surface as bigger copper oxide particles.

Table 1
Textural properties and chemical composition of the synthesized mesoporous molecular sieves.

Sample	Cu content (wt.%)[a]	S_{BET} (m^2/g)[b]	V_{TP} (cm^3/g)[c]	V_{MPP} (cm^3/g)[d]	w_p (nm)[e]	a_o (nm)[f]	t_w (nm)[g]
MCM-41	–	1190	0.57	0.54	3.5	4.08	0.6
Cu-TIE(1%)	0.89	1125	0.97	0.79	3.8	4.38	0.6
Cu-TIE(2%)	1.45	1030	0.95	0.70	3.8	4.44	0.6
Cu-TIE(5%)	3.55	905	1.12	0.48	3.7	4.58	0.9

[a] In the final solid, determined by AA.
[b] Determined by BET.
[c] V_{TP}: total pore volume determined at p/p° = 0.98.
[d] V_{MPP}: primary mesopores volume, obtained by the α_S-plot method.
[e] w_p: pore width.
[f] $a_o = (2/\sqrt{3})d_{100}$.
[g] $t_w = a_0 - w_p$.

The XPS and Auger spectra of the calcined solids and the reduced Cu-TIE(5%) sample are presented in Fig. 3. For all the calcined samples (Fig. 3A, a–c), two peaks centered at about 933.3 eV and 953 eV, corresponding to $Cu2p_{3/2}$ and $Cu2p_{1/2}$ respectively, can be observed. The presence of the shake-up satellite at about 942 eV and the binding energy of $Cu2p_{3/2}$ at 933.3 eV are characteristic of copper in an oxidation state of 2+ [28]. Moreover, in order to confirm this signal assignment, the sample with the highest copper content was reduced in H_2/Ar (5%) flow at 523.15 K for 10 min. Next, ultra-high vacuum was applied for two hours before analyzing. As it can be observed, the binding energy of $Cu2p_{3/2}$ in the reduced sample was lower (932.1 eV) and the satellite lines disappeared, which shows that all copper present in the solid surface was reduced to Cu^+ or Cu°. To distinguish these last two species, the Auger spectrum of the reduced sample was studied. Fig. 3B (d) shows only one CuLMM Auger kinetic energy peak centered at 918.9 eV which corresponds to Cu° [29]. Therefore, using the Auger spectrum of the Cu-TIE(5%) reduced sample as reference, the corresponding spectra of the calcined samples were analyzed. In Fig. 3B (a–c) a peak at about 917.7 eV can be identified as the CuLMM Auger kinetic peak of Cu^{2+} [30]. Thus, these results indicate that the copper in the surface of the synthetized samples is present mainly as Cu^{2+} species.

The UV–vis-DR spectra of the investigated samples are shown in Fig. 4. Between 200 nm and 900 nm, all solids exhibit an intense absorption band that can be decomposed into three contributions, each assigned to a different copper species present in the sample [23]. The first signal, whose maximum is positioned between 310 nm and 350 nm can be associated to the metal-ligand charge transfer $Cu^{2+} \longleftarrow O^{2-}$, that is to isolated 2+ cations (Cu^{2+}) in coordination with oxygen from the network [31]. The silanol groups can stabilize the isolated cations on the support surface up to its saturation. Once this limit is reached, oligomerization begins to occur by aggregation of $Cu^{2+}O^{2-}$ species. This process leads to the formation of linear oligonuclear clusters where copper has a low coordination number [32,33]. The nanoclusters could be stabilized inside the mesoporous channels due to a charge decompensation caused in the siliceous structure by the incorporation of isolated species [34]. These nanoclusters can be assigned to the band located between 400 nm and 600 nm. Finally, the $Cu^{2+}O^{2-}$ aggregation process culminates with the formation of oxide species such as nanoparticles large enough to be observed by XRD at a high angle. CuO presents an absorption band at approximately 750 nm corresponding to

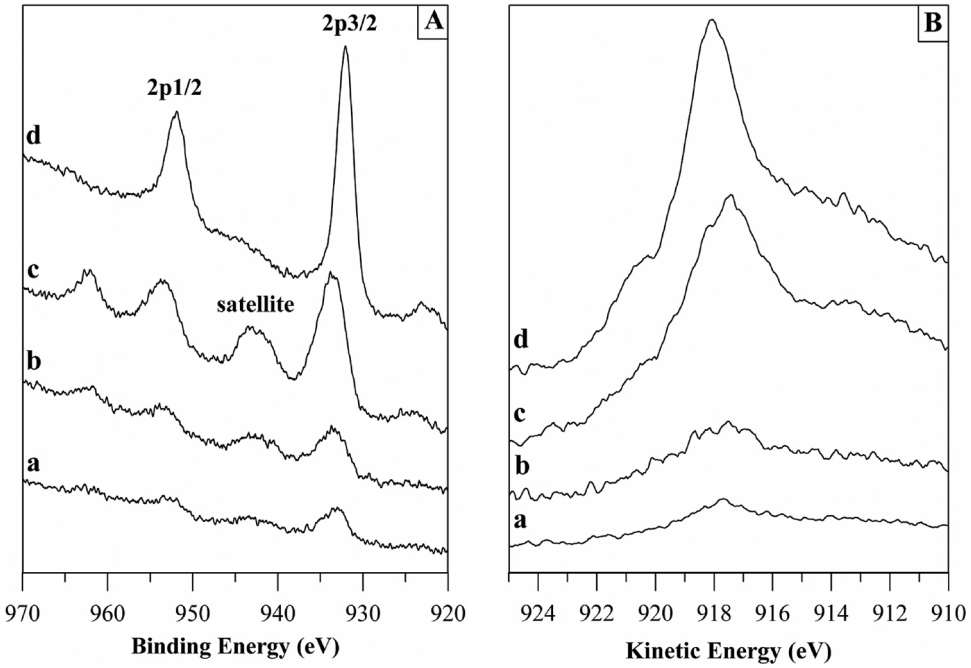

Fig. 3. **A**: Cu2p spectra and **B**: Auger kinetic energy of **a:** calcined Cu-TIE(1%), **b:** calcined Cu-TIE(2%), **c:** calcined Cu-TIE(5%), **d:** reduced Cu-TIE(5%).

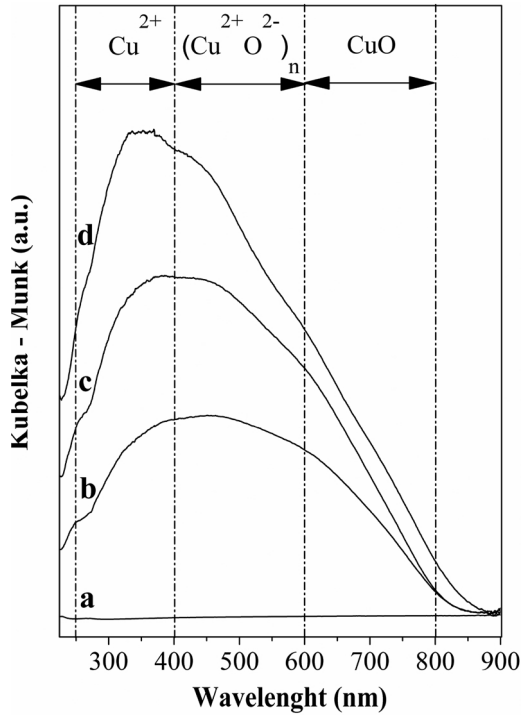

Fig. 4. UV–vis-DR spectra of the synthesized samples with different Cu contents, **a**: MCM-41, **b**: Cu-TIE(1%), **c**: Cu-TIE(2%), **d**: Cu-TIE(5%).

a $^2E_g \rightarrow {}^2T_{2g}$ spin transition of Cu^{2+} with octahedral symmetry [35]. Thus, the last maximum located between 600 nm and 800 nm could be associated to d-d transitions of copper with tetragonally distorted octahedral symmetry. It is known that UV–vis-DR absorption bands can move towards shorter wavelengths when the size of the species decreases indicating a size quantum effect [36]. The relative position of the last contribution regarding bulk CuO would be giving account for this effect. Each sample spectrum has been decomposed according to the mentioned signals. Fig. 5 (A, B, and C) show the results of the deconvolution process, and Fig. 6 presents the relative distribution and chemical composition in wt.% of the species present in the synthesized solids. The wt.% of the Cu species in the different samples was estimated multiplying the overall Cu content in the solid by the % area of each band assigned to the corresponding copper specie as a result of the deconvolution process (the % area of each band was calculated regarding to the total area of the spectrum). As it can be noted in this last figure, the copper species distribution in % area does not change significantly for the different samples. However, when the total metallic content increases, so it does the wt.% of each species. Thus, the Cu-TIE (5%) material exhibits the greatest amount of nanoclusters and exposed copper oxide nanoparticles, which could block some of the isolated Cu^{2+} cations and cause a decrease in S_{BET} as it was already observed from the N_2 adsorption-desorption data.

3.2. Catalytic activity

A series of blank experiments without limonene were conducted to determine the catalyst and temperature effect over the oxidants (H_2O_2 and TBHP). The Cu-TIE(2%) material was selected as a catalyst test for these experiments. Fig. 7 shows the evolution of oxidant conversion over time for each blank experiment. As it can be seen, TBHP is consumed without catalyst at the employed temperature, generating *t*-butanol and molecular oxygen. These results can be explained taking into account that TBHP decomposes homolytically following a free radical mechanism [9]. In the case of H_2O_2, the corresponding profile shows no oxidant conversion. Thus, H_2O_2 does not decompose at the evaluated temperature. These findings could be related to the higher activation energy of the O—O bond in the H_2O_2 molecule concerning to TBHP [5]. When the Cu-TIE(2%) material was added to the reaction medium, the rate of decomposition for both oxidants was accelerated reaching a value over 90% after 5 h. This indicates that under the employed conditions, the copper modified material could be acting as an initiator catalyzing the radical generation process [5].

The values of limonene conversion and selectivity to reaction products at 5 h in the presence/absence of the Cu-TIE(2%) material, for both oxidants are shown in Table 2. For TBHP, in the presence of the catalyst the olefin conversion reached a value of 19.3%, while without the catalyst only a 3.8% of conversion was achieved. However, in both cases, similar selectivities were obtained. Thus, limonene

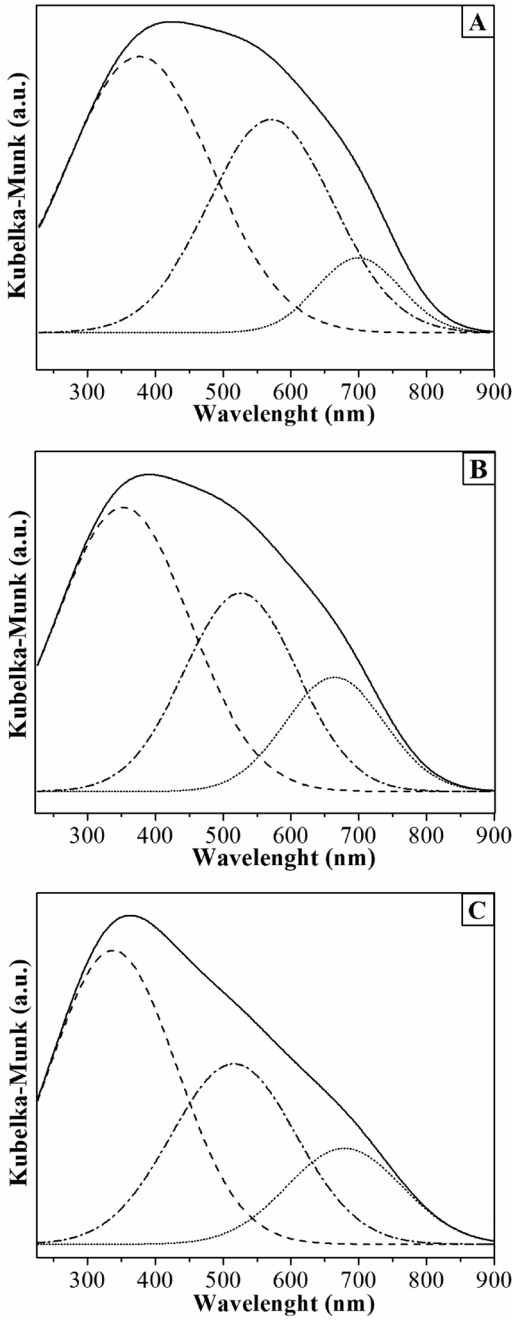

Fig. 5. Deconvoluted spectra of the samples **A:** Cu-TIE(1%), **B:** Cu-TIE(2%) and **C:** Cu-TIE(5%), solid line: final fitted curve, dotted lines: decomposed contributions.

hydroperoxide was found to be the main reaction product with a selectivity of 71.4% and 62.3%, respectively. These results show that the catalyst does not modify the reaction pathway but plays an important role increasing its rate. Other reaction products such as limonene oxide, carvone, carveol, and perillaldehyde were obtained in lower percentages. When H_2O_2 was used as oxidant, the limonene conversion reached a value of 8.5% in the presence of catalyst. Limonene oxide, limonene diepoxide, and glycol were obtained with a selectivity of 58.7%. The remaining 41.3% included carveol, carvone, perillaldehyde, and limonene hydroperoxide. Meanwhile, the reaction without catalyst showed a very low limonene conversion (1%). Therefore, in the case of H_2O_2 the presence of the copper modified mesoporous sieve is necessary to initiate the oxidation process.

Analyzing the activity of the catalyst for both oxidants, a different

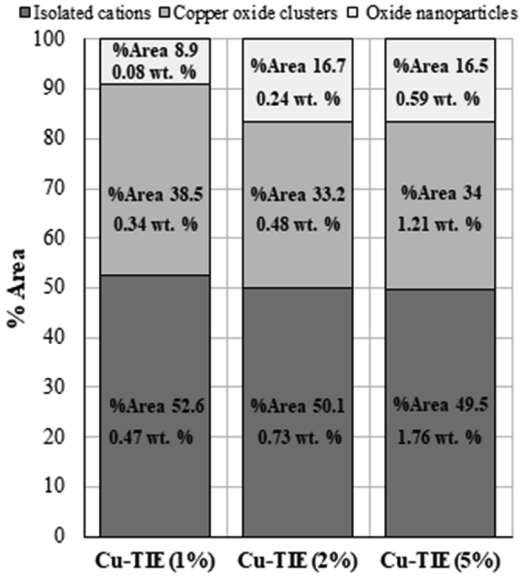

Fig. 6. Chemical composition and Cu species relative distribution in the Cu-TIE (x) samples.

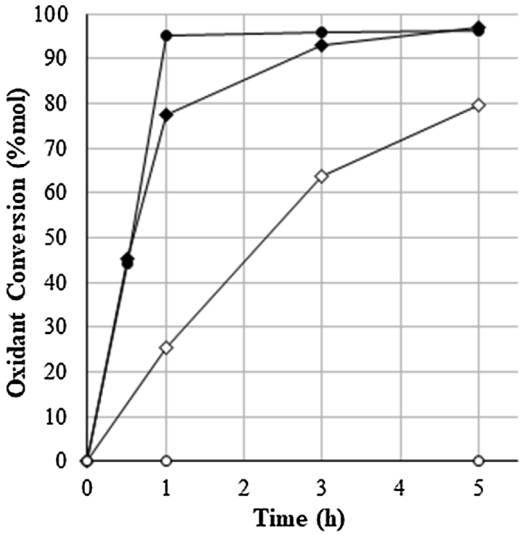

Fig. 7. Oxidant conversion vs. reaction time: (●) H_2O_2 with catalyst, (○) H_2O_2 without catalyst, (♦) TBHP with catalyst, (◊) TBHP without catalyst. Reaction conditions: Cu-TIE(2%) = 100 mg, temperature = 343 K, solvent: AcN, reaction time = 5 h.

distribution of products can be observed (Table 2). To explain the obtained differences, the mechanism shown in Scheme 1 is proposed as a possible reaction pathway when TBHP is used with Cu-MCM for limonene oxidation.

Copper acts as an electron-transfer catalyst and a redox initiator in a one-electron step, where the oxidation state of the metal varies between 2+ and 1+ generating free radicals. Thus Cu^{2+} isolated species present in the modified mesoporous molecular sieve could be the responsible for accelerating the radical chain initiation step producing alkoxyl (tBuO•) and alkylperoxyl (tBuO$_2^{\bullet}$) radicals. Moreover, the temperature produces also hydroxyl (HO•) radicals by homolytic cleavage of the TBHP (tBuO$_2$H) O—O bond. In step **(a)**, the generated alkoxyl and hydroxyl radicals are able to abstract an allylic hydrogen from a limonene molecule to yield a limonene radical (L•) and t-butanol (tBuOH) or water respectively. Step **(b)** shows how the interaction of L• with molecular oxygen affords a LOO• radical. Then, a hydrogen is transferred from the limonene substrate to the LOO• radical yielding the

Table 2
Limonene oxidation with TBHP and H_2O_2.

Oxidant		X_{Lim} (% mol)	Selectivity (%)						
			Limonene Oxide	Limonene Diepoxide	Limonene Glycol	Carveol	Carvone	Perillaldehyde	Limonene Hydroperoxide
TBHP	Without catalyst	3.8	8.6	0.0	0.0	8.6	6.7	13.8	62.3
	With catalyst	19.3	6.7	0.0	0.0	5.3	5.1	11.6	71.4
	With catalyst [a]	9.5	6.8	0.0	0.0	0.0	5.9	12.9	74.4
	With catalyst [b]	10.0	7.5	0.0	0.0	0.0	5.8	13.9	72.8
H_2O_2	Without catalyst	1	75.2	0.0	0.0	24.8	0.0	0.0	0.0
	With catalyst	8.5	37.2	15.9	5.6	13.1	7.2	9.1	11.9

Reaction conditions: Limonene/Oxidant molar ratio = 2, Cu-TIE(2%) = 100 mg, temperature = 343 K, solvent: AcN, reaction time = 5 h.
[a] With BHT (8% of the initial limonene mmols), added at the beginning of the reaction.
[b] Employing N_2 atmosphere.

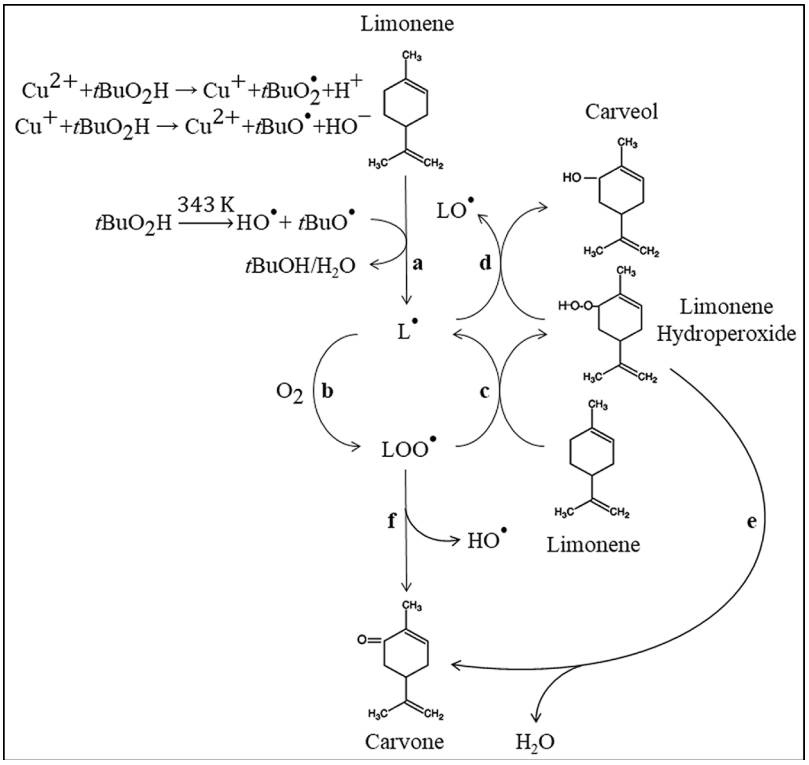

Scheme 1. Proposed reaction mechanism for limonene oxidation with TBHP catalyzed by Cu-TIE(x).

limonene hydroperoxide (LOOH) and another L˙ radical, step **(c)**. Next, limonene hydroperoxide can undergo consecutive co-oxidation to afford carveol and carvone, steps **(d)** and **(e)** respectively. In addition, carvone can also be obtained through step **(f)**. Moreover perillaldehyde, not shown in Scheme 1, was obtained by allylic oxidation at the position 7 of the limonene molecule. Perillyl alcohol was not detected as a reaction product, which indicates that perillaldehyde can be obtained directly from limonene and not via alcohol. This observation is in agreement with results reported by Naróg et al. [37]. Additionally, limonene oxide was obtained with a selectivity of 6.7%. Its formation can be interpreted considering that alkylperoxyl radicals (LOO• and tBuO$_2^•$) can be added to the C=C double bond to afford limonene oxide (LO) (Eqs. (5) and (6)).

$$LOO^• + L \rightarrow LO + LO^• \quad (5)$$

$$t\mathrm{BuO}_2^• + L \rightarrow LO + t\mathrm{BuO}^• \quad (6)$$

While abstraction of an allylic hydrogen and addition of a radical specie to the C=C double bond are competing processes in olefin oxidations [5,38,39], in this system, allylic products (limonene hydroperoxide, carveol, carvone, and perillaldehyde) were favored with a total selectivity of 93.4%. These results can be explained taking into account that LOO• and tBuO$_2^•$ are bulkier radicals, thus their approach to the double bond of limonene is hindered and allylic oxidation is favored. Finally, additional amounts of carvone (L=O) and carveol (LOH) can be afforded through Eqs. (7) to (11).

$$LO^• + O_2 \rightarrow L{=}O + HO_2^• \quad (7)$$

$$LO^• + L \rightarrow L^• + LOH \quad (8)$$

$$HO^• + L^• \rightarrow LOH \quad (9)$$

$$t\mathrm{BuO}_2^• + L^• \rightarrow L{=}O + t\mathrm{BuOH} \quad (10)$$

$$2\,LOO^• \rightarrow LOH + L{=}O + O_2 \quad (11)$$

In order to further confirm the proposed mechanism, a new reaction was carried out employing BHT as radical scavenger. A small amount of BHT was added together with the catalyst at the beginning of the reaction. Fig. 8 compares the behavior of limonene conversion over time for a typical reaction with TBHP and the one with the radical scavenger.

As it can be noted, during the first hour in the presence of BHT, the

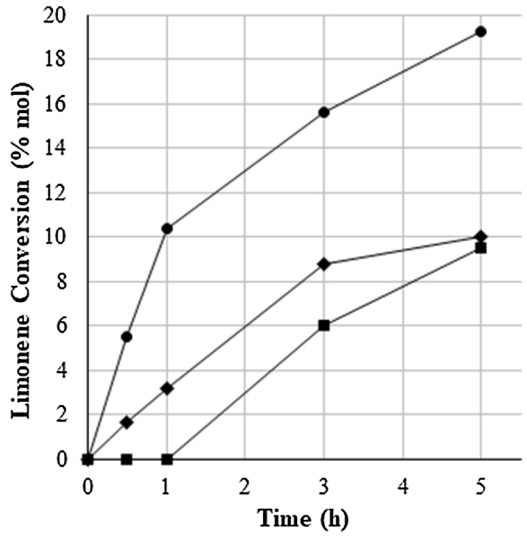

Fig. 8. Limonene conversion vs. reaction time: (●) Typical reaction, (♦) N_2 atmosphere, (■) with BHT. Reaction conditions: Oxidant - TBHP, Limonene/TBHP molar ratio = 2, Cu-TIE(2%) = 100 mg, temperature = 343 K, solvent: AcN, reaction time = 5 h.

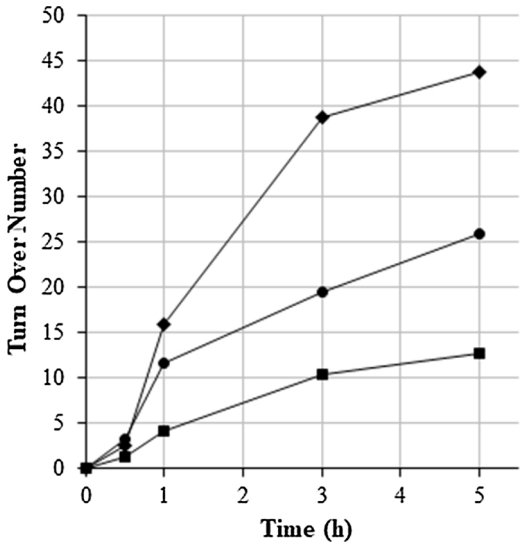

Fig. 9. TON vs. reaction time: (♦) Cu-TIE(1%), (●) Cu-TIE(2%), (■) Cu-TIE (5%). Reaction conditions: Oxidant - H_2O_2, Limonene/H_2O_2 molar ratio = 2, catalyst = 100 mg, temperature = 343 K, solvent: AcN, reaction time = 5 h.

reaction was stopped, and no product was formed. Then, after the BHT was completely consumed, the radical reaction began. Product distribution after 5 h (Table 2) showed similar behavior to the typical reaction, obtaining around a 70% in selectivity to limonene hydroperoxide. This indicates that all products are formed through a radical mechanism. Furthermore, the reaction was tested under nitrogen atmosphere obtaining a limonene conversion considerably lower than the typical reaction, without changes in selectivity (Fig. 8, Table 2). This indicates that molecular oxygen plays an important role in the radical chain propagation. Hence, the reaction proceeds through the oxidation mechanism described above.

On the other hand, the obtained products distribution with H_2O_2 and Cu-TIE(2%) (Table 2) can be explained according to the mechanism shown in Scheme 2.

Like it was proposed for TBHP, the oxidant (HO_2H) activation by Cu^{2+} isolated species present in the mesoporous molecular sieve

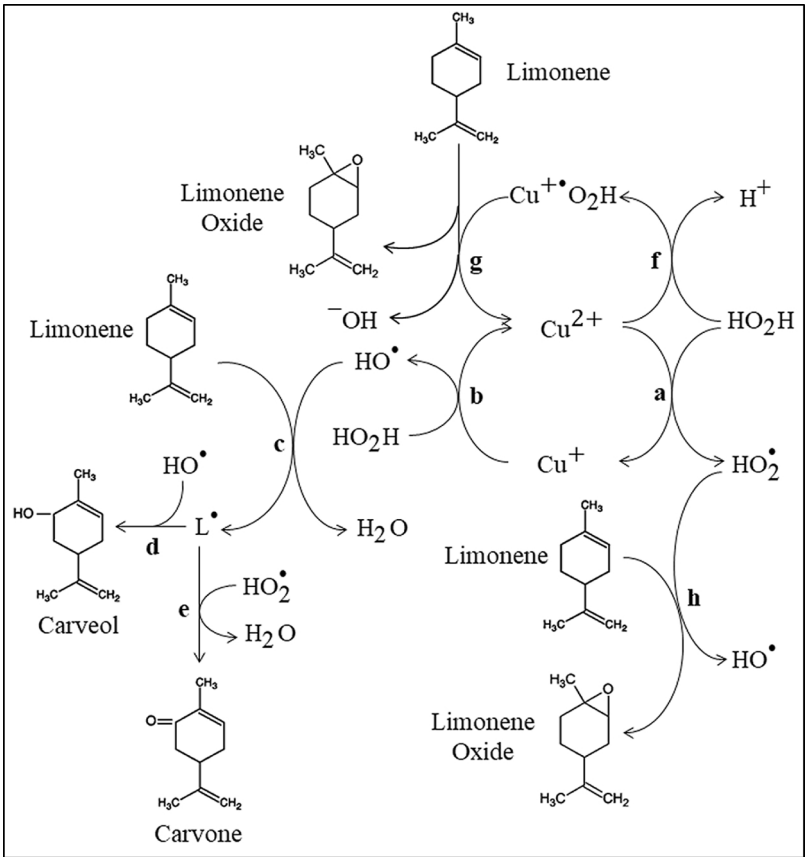

Scheme 2. Proposed reaction mechanism for limonene oxidation with H_2O_2 catalyzed by Cu-TIE(x).

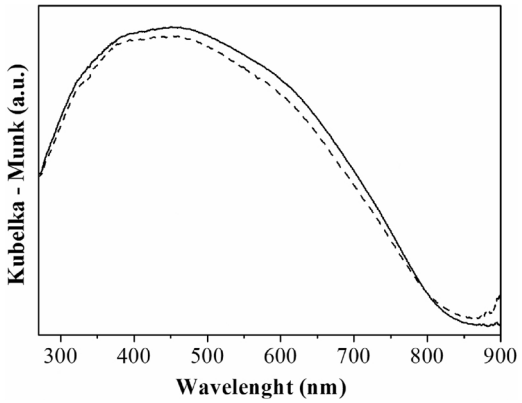

Fig. 10. UV–vis-DR of the fresh and used Cu-TIE(1%) material, solid line: fresh Cu-TIE(1%), dotted line: used Cu-TIE(1%).

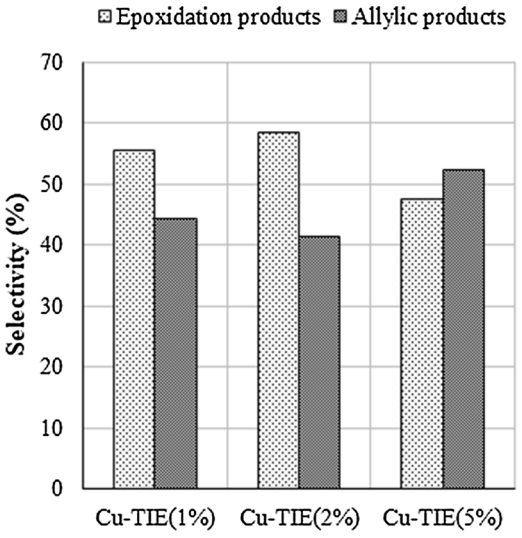

Fig. 11. Selectivity to reaction products after 5 h over Cu-TIE(x). Reaction conditions: Oxidant - H_2O_2, Limonene/H_2O_2 molar ratio = 2, catalyst = 100 mg, temperature = 343 K, solvent: AcN, reaction time = 5 h.

produces peroxyl ($HO_2^{\bullet}$) and hydroxyl ($HO^{\bullet}$) radicals, steps **(a)** and **(b)** [40]. As it was already discussed, $HO^{\bullet}$ radicals can subtract an allylic hydrogen from the olefin and generate a $L^{\bullet}$ radical (step **c**). Then, $L^{\bullet}$ can form carveol and carvone trough steps **(d)** and **(e)** respectively. Additionally, a H_2O_2 molecule could coordinate to a Cu^{2+} isolated site in the catalyst to yield the $Cu^{+\bullet}O_2H$ specie, step **(f)** [41,42]. Next, oxygen transfer to a limonene molecule would yield the corresponding oxide as main product, step **(g)**. At the same time, it cannot be excluded that addition of peroxyl radicals to the olefin C=C double bond could afford limonene oxide as shown in step **(h)** [39,43]. Moreover, limonene diepoxide was obtained as a result of both double bonds oxidation, while glycol was formed by the epoxide ring opening in the presence of water [44,45]. Limonene hydroperoxide was also obtained in low quantities from Eq. (12). Finally, peroxyl and hydroxyl radicals can recombine through processes shown in Eqs. (13) and (14).

$$HO_2^{\bullet} + L^{\bullet} \rightarrow LOOH \quad (12)$$

$$HO^{\bullet} + HO^{\bullet} \rightarrow HO_2H \quad (13)$$

$$HO_2^{\bullet} + HO^{\bullet} \rightarrow H_2O + O_2 \quad (14)$$

Taking into account that the obtained main products in the oxidation of limonene with H_2O_2 have industrial relevance, the performance of Cu-TIE(1%) and Cu-TIE(5%) as catalysts was evaluated employing this oxidant. Fig. 9 shows the evolution of TON vs. time for all the synthesized materials under typical reaction conditions. Cu-TIE(1%) presents the highest TON values, thus this material shows the best catalytic performance of the three synthesized samples. The TON values observed for the lower metallic content solid could be giving account for the high activity of the Cu^{2+} cations dispersed in the network. It is interesting to note that the proportion of these active species is maintained after 5 h of reaction. This is evidenced by the shapes of the fresh and used Cu-TIE(1%) sample UV–vis-DR spectra, which do not show significant changes (Fig. 10).

Fig. 11 presents the product selectivity after 5 h of reaction employing H_2O_2 and the Cu-TIE(x) materials. The compounds obtained from the oxidation of the double bonds are presented as epoxidation products, they include limonene oxide, limonene diepoxide, and glycol. Meanwhile, carveol, carvone, perillaldehyde, and limonene hydroperoxide were considered within the allylic products category.

It was found that over Cu-TIE(1%) and Cu-TIE(2%) catalysts, epoxidation products were favored over allylic products. Meanwhile, with Cu-TIE(5%), selectivity to allylic products increased. This is likely due to differences in the species distribution present in the materials. Cu-TIE(5%) exhibited the greatest amount of nanoclusters and exposed copper oxide species, as it was observed by UV–vis-DR. Moreover, as it was previously discussed from the N_2 adsorption-desorption results, these species could be blocking some of the support pores and thus some of the isolated Cu^{2+} sites partly responsible for limonene oxide generation. Consequently, the nanoclusters and/or copper oxide species more exposed than the isolated Cu^{2+} sites, could be involved in the generation of hydroxyl radicals through their interaction with H_2O_2. In this sense, Abdullah et al. [46] found that hydroxyl radicals can be produced by the decomposition of H_2O_2 catalyzed by CuO. Additionally, Wang and Valentine [47] and Kitajima et al. [48] also reported the decomposition of this oxidant by several metal oxides. Then, when Cu-TIE(5%) was used the formation of free radicals could be favored increasing allylic product selectivity.

4. Conclusions

The mesoporous molecular sieves Cu-TIE(1%), Cu-TIE(2%) and Cu-TIE(5%) were successfully synthesized employing the template-ion exchange method. All solids exhibited good structural regularity and high mesoporosity. Unlike Cu-TIE(1%) and Cu-TIE(2%) samples, Cu-TIE (5%) presented a small secondary mesoporosity likely related to Cu content. The presence of copper in oxidation state 2+ could be inferred by XPS. The analysis of the UV–vis-DR spectra showed that the increase in metallic content favors the formation of nanoclusters and exposed copper oxide species.

The Cu-TIE(2%) solid was active in the limonene oxidation reaction employing TBHP and H_2O_2 as oxidants. In both cases, the copper modified material activated the oxidants through free radical generation. Furthermore, under the employed reaction conditions, homolytic cleavage of the O—O bond was observed for TBHP. With this oxidant, limonene hydroperoxide was found to be the main reaction product obtained, meanwhile using H_2O_2 epoxidation products were formed in greater amounts.

Employing H_2O_2 with the Cu-TIE(1%) and Cu-TIE(2%) materials, epoxidation products were favored over allylic products. Whereas that with Cu-TIE(5%), selectivity to allylic products increased. Therefore, limonene oxidation using H_2O_2 over Cu-TIE(x) mesoporous materials with low metal content is proposed as a plausible combination to obtain high added value oxygenated derivatives as main reaction products.

Acknowledgements

The authors would like to thank CONICET and UTN-FRC for their financial support, as well as Mr. Cacace Ruiz C., Geol. Fernandez J., Mg. Caglieri S., Dra. Cornaglia L. and Lic. Mori M.F. for their valuable contributions. The authors also thank Martinez M. for the linguistic

contributions.

References

[1] M. Pourbafrani, G. Forgacs, I.S. Horvath, C. Niklasson, M.J. Taherzadeh, Production of biofuels, limonene and pectin from citrus wastes, Bioresour. Technol. Rep. 101 (2010) 4246–4250, https://doi.org/10.1016/j.biortech.2010.01.077.

[2] J.A. Becerra, L.M. Gonzalez, A. Villa, A bio-inspired heterogeneous catalyst for the transformation of limonene from orange peel waste biomass into value-added products, Catal. Today 302 (2018) 250–260, https://doi.org/10.1016/j.cattod.2017.07.012.

[3] R. Ciriminna, M. Lomeli-Rodriguez, P. Demma Cará, J.A. Lopez-Sanchez, M. Pagliaro, Limonene: a versatile chemical of the bioeconomy, Chem. Commun. (Camb.) 50 (2014) 15288–15296, https://doi.org/10.1039/c4cc06147k.

[4] A. Wróblewska, E. Makuch, P. Miądlicki, The studies on the limonene oxidation over the microporous TS-1 catalyst, Catal. Today 268 (2016) 121–129, https://doi.org/10.1016/j.cattod.2015.11.008.

[5] R.A. Sheldon, J.K. Kochi, Metal-Catalysed Oxidations of Organic Compounds, Academic Press, New York, 1981.

[6] R.A. Sheldon, New catalytic methods for selective oxidation, J. Mol. Catal. A Chem. 20 (1983) l–26, https://doi.org/10.1016/0304-5102(83)83011-9.

[7] M.V. Cagnoli, S.G. Casuscelli, A.M. Alvarez, J.F. Bengoa, N.G. Gallegos, N.M. Samaniego, M.E. Crivello, G.E. Ghione, C.F. Perez, E.R. Herrero, S.G. Marchetti, "Clean" limonene epoxidation using Ti-MCM-41 catalyst, Appl. Catal. A Gen. 287 (2005) 227–235, https://doi.org/10.1016/j.apcata.2005.04.001.

[8] M.G. Egusquiza, C.I. Cabello, I.L. Botto, H.J. Thomas, S. Casuscelli, E. Herrero, D. Gazzoli, Advance in the study of limonene epoxidation with H_2O_2 catalyzed by Cu(II) complex heteropolytungstates, Catal. Commun. 26 (2012) 117–121, https://doi.org/10.1016/j.catcom.2012.04.030.

[9] L. Charbonneau, S. Kaliaguine, Epoxidation of limonene over low coordination Ti in Ti- SBA-16, Appl. Catal. A Gen. 533 (2017) 1–8, https://doi.org/10.1016/j.apcata.2017.01.001.

[10] A. Wróblewska, The epoxidation of limonene over the TS-1 and Ti-SBA-15 catalysts, Molecules 19 (2014) 19907–19922, https://doi.org/10.3390/molecules191219907.

[11] A. Wróblewska, E. Makuch, P. Miądlicki, The oxidation of limonene at raised pressure and over the various titanium-silicate catalysts, Pol. J. Chem. Technol. 17 (4) (2015) 82–87, https://doi.org/10.1515/pjct-2015-0072.

[12] R. Ciriminna, F. Parrino, C. De Pasquale, L. Palmisano, M. Pagliaro, Photocatalytic partial oxidation of limonene to 1,2 limonene oxide, Chem. Commun. (Camb.) 54 (2018) 1008–1011, https://doi.org/10.1039/c7cc09788c.

[13] J. Młodzik, A. Wróblewska, E. Makuch, R. Wróbel, B. Michalkiewicz, Fe/EuroPh catalysts for limonene oxidation to 1,2-epoxylimonene, its diol, carveol, carvone and perillyl alcohol, Catal. Today 268 (2016) 111–120, https://doi.org/10.1016/j.cattod.2015.11.010.

[14] C.K. Modi, J.A. Chudasama, H.D. Nakum, D.K. Parmar, A.L. Patel, Catalytic oxidation of limonene over zeolite-Y entrapped oxovanadium (IV) complexes as heterogeneous catalysts, J. Mol. Catal. A Chem. 395 (2014) 151–161, https://doi.org/10.1016/j.molcata.2014.08.022.

[15] D.R. Godhani, H.D. Nakum, D.K. Parmar, J.P. Mehta, N.C. Desai, Zeolite-Y immobilized Metallo-ligand complexes: a novel heterogenous catalysts for selective oxidation, Inorg. Chem. Commun. 72 (2016) 105–116, https://doi.org/10.1016/j.inoche.2016.08.017.

[16] N.K. Ojha, G.V. Zyryanov, A. Majee, V.N. Charushin, O.N. Chupakhin, S. Santra, Copper nanoparticles as inexpensive and efficient catalyst: a valuable contribution in organic synthesis, Coord. Chem. Rev. 353 (2017) 1–57, https://doi.org/10.1016/j.ccr.2017.10.004.

[17] Y. Fang, Y. Guo, Copper-based non-precious metal heterogeneous catalysts for environmental remediation, Chin. J. Catal. 39 (2018) 566–582, https://doi.org/10.1016/S18722067(17)629966.

[18] A. Kowalczyk, Z. Piwowarska, D. Macina, P. Kustrowski, A. Rokicinska, M. Michalik, L. Chmielarz, MCM-41 modified with iron by template ion-exchange method as effective catalyst for DeNOx and NH_3-SCO processes, Chem. Eng. J. 295 (2016) 167–180, https://doi.org/10.1016/j.cej.2016.03.049.

[19] A. Kowalczyk, A. Święs, B. Gil, M. Rutkowska, Z. Piwowarska, A. Borcuch, M. Michalik, L. Chmielarz, Effective catalysts for the low-temperature NH_3-SCR process based on MCM-41 modified with copper by template ion-exchange (TIE) method, Appl. Catal. B 237 (2018) 927–937, https://doi.org/10.1016/j.apcatb.2018.06.052.

[20] M. Grün, K.K. Unger, A. Matsumoto, K. Tsutsumi, Novel pathways for the preparation of mesoporous MCM-41 materials: control of porosity and morphology, Microporous Mesoporous Mater. 27 (1999) 207–216, https://doi.org/10.1016/S1387-1811(98)00255-8.

[21] X. Liu, H. Sun, Y. Yang, Rapid synthesis of highly ordered Si-MCM-41, J. Col. Int. Sci. 319 (2008) 377–380, https://doi.org/10.1016/j.jcis.2007.11.025.

[22] V.R. Elías, M.C. Crivello, E.R. Herrero, S.G. Casuscelli, G.A. Eimer, Some considerations to optimize the synthesis procedure and the structural quality of mesostructured silicas, J. Non-Cryst. Solids 355 (2009) 1269–1273, https://doi.org/10.1016/j.jnoncrysol.2009.04.019.

[23] C.M. Chanquía, A.L. Cánepa, J. Bazán-Aguirre, K. Sapag, E. Rodríguez-Castellón, P. Reyes, E.R. Herrero, S.G. Casuscelli, G.A. Eimer, Copper-containing spherical mesoporous silicates prepared by template-ion exchange: a multitechnique characterization and oxidation properties, Microporous Mesoporous Mater. 151 (2012) 2–12, https://doi.org/10.1016/j.micromeso.2011.07.001.

[24] Y. Wang, Q. Zhang, Y. Ohishi, T. Shishido, K. Takehira, Synthesis of V-MCM-41 by template-ion exchange method and its catalytic properties in propane oxidative dehydrogenation, Catal. Lett. 72 (3-4) (2001) 215–219, https://doi.org/10.1023/A:1009001707280.

[25] Y.J. Do, J.H. Kim, J.H. Park, S.S. Park, S.S. Hong, C.S. Suh, G.D. Lee, Photocatalytic decomposition of 4-nitrophenol on Ti-containing MCM-41, Catal. Today 101 (2005) 299–305, https://doi.org/10.1016/j.cattod.2005.03.009.

[26] G.A. Eimer, S.G. Casuscelli, C.M. Chanquía, V.R. Elías, M.E. Crivello, E.R. Herrero, The influence of Ti-loading on the acid behavior and on the catalytic efficiency of mesoporous Ti-MCM-41 molecular sieves, Catal. Today 133–135 (2008) 639–646, https://doi.org/10.1016/j.cattod.2007.12.096.

[27] S. Meghana, P. Kabra, S. Chakraborty, N. Padmavathy, Understanding the pathway of antibacterial activity of copper oxide nanoparticles, R. Soc. Chem. 5 (2015) 12293–12299, https://doi.org/10.1039/c4ra12163e.

[28] K. Yoshida, C. Gonzalez-Arellano, R. Luque, P.L. Gai, Efficient hydrogenation of carbonyl compounds using low-loaded supported copper nanoparticles under microwave irradiation, Appl. Catal. A-Gen. 379 (2010) 38–44, https://doi.org/10.1016/j.apcata.2010.02.028.

[29] Z. Huang, F. Cui, H. Kang, J. Chen, X. Zhang, C. Xia, Highly dispersed silica-supported copper nanoparticles prepared by precipitation-gel method: a simple but efficient and stable catalyst for glycerol hydrogenolysis, Chem. Mater. 20 (2008) 5090–5099, https://doi.org/10.1021/cm8006233.

[30] R. Cousin, E. Abi-Aad, S. Capelle, D. Courcot, J.F. Lamonier, A. Aboukaıs, Physico-chemical study of impregnated Cu and V species on CeO_2 support by thermal analysis, XRD, EPR, ^{51}V-MAS-NMR and XPS, J. Mater. Sci. 42 (2007) 6188–6196, https://doi.org/10.1007/s10853-006-1165-6.

[31] H. Praliaud, S. Mikhailenko, Z. Chajar, M. Primet, Surface and bulk properties of Cu-ZSM-5 and Cu/Al_2O_3 solids during redox treatments. Correlation with the selective reduction of nitric oxide by hydrocarbons, Appl. Catal. B 16 (1998) 359–374, https://doi.org/10.1016/S0926-3373(97)00093-3.

[32] V. Elías, E. Sabre, K. Sapag, S. Casuscelli, G. Eimer, Influence of the Cr loading in Cr/MCM-41 and TiO2/Cr/MCM-41 molecular sieves for the photodegradation of Acid Orange 7, Appl. Catal. A Gen. 413-414 (2012) 280–291, https://doi.org/10.1016/j.apcata.2011.11.019.

[33] N. Cuello, V. Elías, S. Urreta, M. Oliva, G. Eimer, Microstructure and magnetic properties of iron modified mesoporous silica obtained by one step direct synthesis, Mater. Res. Bull. 48 (2013) 3559–3563, https://doi.org/10.1016/j.materresbull.2013.05.065.

[34] C.M. Chanquía, K. Sapag, E. Rodríguez-Castellón, E.R. Herrero, G.A. Eimer, Nature and location of copper nanospecies in mesoporous molecular sieves, J. Phys. Chem. C 114 (2010) 1481–1490, https://doi.org/10.1021/jp9094529.

[35] S. Velu, L. Wang, M. Okazaki, K. Suzuki, S. Tomura, Characterization of MCM-41 mesoporous molecular sieves containing copper and zinc and their catalytic performance in the selective oxidation of alcohols to aldehydes, Microporous Mesoporous Mater. 54 (2002) 113–126, https://doi.org/10.1016/S1387-1811(02)00358-X.

[36] N.I. Cuello, V.R. Elías, C.E. Rodriguez Torres, M.E. Crivello, M.I. Oliva, G.A. Eimer, Development of iron modified MCM-41 as promising nano-composites with specific magnetic behavior, Microporous Mesoporous Mater. 203 (2015) 106–115, https://doi.org/10.1016/j.micromeso.2014.10.005.

[37] D. Naróg, A. Szczepanik, A. Sobkowiak, Iron(II, III)-Catalyzed oxidation of limonene by dioxygen, Catal. Lett. 120 (2008) 320–325, https://doi.org/10.1007/s10562-007-9290-7.

[38] R.A. Sheldon, J.A. Van Doorn, Metal-catalyzed epoxidation of olefins with organic hydroperoxides: I. A comparison of various metal catalysts, J. Catal. 31 (1973) 427–437, https://doi.org/10.1016/0021-9517(73)90314-X.

[39] S. Stahl, P. Alsters, Liquid Phase Aerobic Oxidation Catalysis - Industrial Aplications and Accademic Perspectives, Wiley-VCH, USA, 2016.

[40] A.D. Bokare, W. Choi, Review of iron-free Fenton-like systems for activating H_2O_2 in advanced oxidation processes, J. Hazard. Mater. 275 (2014) 121–135, https://doi.org/10.1016/j.jhazmat.2014.04.054.

[41] A.L. Cánepa, C.M. Chanquía, G.A. Eimer, S.G. Casuscelli, Oxidation of olefins employing mesoporous molecular sieves modified with copper, Appl. Catal. A Gen. 462-463 (2013) 8–14, https://doi.org/10.1016/j.apcata.2013.04.031.

[42] G. Zhang, J. Long, X. Wang, Z. Zhang, W. Dai, P. Liu, Z. Li, L. Wu, X. Fu, Catalytic role of Cu sites of Cu/MCM-41 in phenol hydroxylation, Langmuir 26 (2) (2010) 1362–1371, https://doi.org/10.1021/la902436s.

[43] A.J. Bonon, Y.N. Kozlov, J.O. Bahú, R. Maciel Filho, D. Mandelli, G.B. Shul'pin, Limonene epoxidation with H_2O_2 promoted by Al_2O_3: kinetic study, experimental design, J. Catal. 319 (2014) 71–86, https://doi.org/10.1016/j.jcat.2014.08.004.

[44] A.L. Cánepa, V.R. Elías, V.M. Vaschetti, E.V. Sabre, G.A. Eimer, S.G. Casuscelli, Selective oxidation of benzyl alcohol through eco-friendly processes using mesoporous V-MCM-41, Fe-MCM-41 and Co-MCM-41 materials, Appl. Catal. A Gen. 545 (2017) 72–78, https://doi.org/10.1016/j.apcata.2017.07.039.

[45] A.L. Cánepa, C.M. Chanquía, V.M. Vaschetti, G.A. Eimer, S.G. Casuscelli, Biomass toward fine chemical products: oxidation of α-pinene over sieves nanostructured modified with vanadium, J. Mol. Catal. A Chem. 404 (2015) 65–73, https://doi.org/10.1016/j.molcata.2015.04.009.

[46] A.H. Abdullah, W.Y. Wong, M.I. Yaziz, Decolorization of reactive orange 16 dye by copper oxide system, Sains Malays. 39 (4) (2010) 587–591.

[47] A.H. Wang, R.L. Valentine, Hydrogen peroxide decomposition kinetics in the presence of iron oxides, in: W.W. Eckenfelder, W.W. Bowers, J.A. Roth (Eds.), In Chemical Oxidation 3. Technologies for the Nineties, Technomic Publishing AG, Basel, 1994, pp. 74–79.

[48] N. Kitajima, S. Fukuzumi, Y. Ono, Formation of superoxide ion during the decomposition of hydrogen peroxide on supported metal oxides, J. Phys. Chem. 82 (13) (1978) 1505–1509, https://doi.org/10.1021/j100502a009.